MICROWAVE RADIATION CHARACTERISTICS OF GLACIAL ICE OBSERVED BY AMSR-E

Hyangsun Han and Hoonyol Lee

Department of Geophysics, Kangwon National University (hyangsun@kangwon.ac.kr, hoonyol@kangwon.ac.kr)

ABSTRACT ... Sea ice concentration (SIC) calculated from the AMSR-E sensor onboard Aqua satellite by using NASA Team2 (NT2) algorithm has proven to be very accurate over sea ice of type A, B and C in Antarctic Ocean. When icebergs and ice shelves originated from glacial (fresh water) ice are dominant in an AMSR-E footprint, the accuracy of NT2 algorithm is not well maintained and a new algorithm may be necessary to accommodate the microwave radiation characteristics of glacial ice. We extracted the concentrations of sea ice and glacial ice from two ENVISAT ASAR images of George V Coast in the southern Antarctica, and compared them with AMSR-E NT2 SIC. The result showed that the NT2 algorithm underestimates the concentration of glacial ice on icebergs and ice shelf by 27.8% and 23.3%, respectively. We also found that glacial ice occupies a unique region in the *PR* (polarization ratio) and *GR* (spectral gradient ratio) domain different from other types of ice such as ice type A, B, and C, and open water. This implies that *glacial ice concentration* can be added as a new category of ice to the NT2 algorithm.

KEY WORDS: glacial ice, iceberg, ice shelf, sea ice concentration, AMSR-E, NASA Team2 algorithm

1. INTRODUCTION

When snow is precipitated, accumulated and compressed on land for a long time, glacial ice is formed to appear as ice sheets, ice shelves, glaciers, and icebergs. Originated from fresh water, glacial ice has different physical properties from sea ice frozen from salty water (Han and Lee, 2007). Due to high pressure, air bubbles are compressed to be small enough to cause Rayleigh scattering so that most glacial ice looks blue. The size of ice crystals is very large due to slow recrystallization process, especially in polar region (Haykin *et al*., 1994). As the global warming is accelerated, large quantities of the glacial ice are flowed into ocean that changes coastal landform and the environment of sea ice formation. It is very important to detect discharge rate of glacial ice by observing icebergs floating at sea effectively for the study of mass-balance of polar ice, not to mention the navigational safety issue.

Satellite passive microwave (PM) sensors are widely used to study the polar ice. Although satellite PM sensors have relatively low spatial resolution of tens of km when compared to active radar, they have excellent temporal resolution so that they can provide daily sea ice concentration (SIC) over Arctic and Antarctic ocean (Markus and Cavalieri, 2000). Advanced Microwave Scanning Radiometer-EOS (AMSR-E) is a typical PM sensor which provides SIC using NASA Team2 (NT2) algorithm.

The NT2 algorithm with AMSR-E has better spatial resolution (12.5 km) and accuracy of SIC than NASA Team (NT) algorithm (Cavalieri *et al*., 1997) with Special Sensor Microwave/Imager (SSM/I) data. Many studies on NT2 SIC have been performed to calibrate and validate the SIC product. Cavalieri *et al* (2006) evaluated the AMSR-E NT2 SIC by using airborne SAR and Landsat-7 ETM+ images. They found that AMSR-E underestimates SIC when snow is heaped over sea ice. Lee and Han (2008) compared Korea Multi-Purpose Satellite-1 (KOMPSAT-1) Electronic Optical Camera (EOC) images with the AMSR-E NT2 SIC. They reported that dark-grey ice, which is undetectable by SSM/I NT algorithm, can be account for by AMSR-E NT2 algorithm.

Polar ice has various physical properties according to ice type, thickness, moisture content, and snow on ice surface (Andersen *et al*., 2007). Consequently, glacial ice has different radiation properties from sea ice and open water. Sea ice algorithms did not accounted for the effect of glacial ice so far.

In this study, we used ENVISAT Advanced Synthetic Aperture Radar (ASAR) images and a series of MODIS images to identify sea ice, icebergs, and ice shelf near the George V Coast in the southern Antarctica, and compared them with AMSR-E NT2 SIC. We then evaluated the accuracy and the effect of glacial ice on AMSR-E NT2 SIC. We also analyzed the characteristics of microwave radiation of glacial ice and compared it with those of sea ice and open water.

2. THE EFFECT OF GLACIAL ICE ON NT2 SIC

We used two ENVISAT ASAR images obtained over the George V Coast in the southern Antarctica adjacent to the Pacific Ocean on 20 and 26 April, 2006 (Table 1). In the ASAR images, most sea surface was covered with sea ice and there are several icebergs and an ice shelf (Fig. 1a). The distinction between sea ice and ice shelf was difficult by ASAR images alone, but we could confirm the ice shelf region through time-series MODIS images (Fig. 2).

We masked inland in the ASAR images using the land mask product of the NT2 algorithm and classified ice type into sea ice, icebergs, and ice shelf by supervised

Table 2. ENVISAT ASAR images used in this study.

Date	Mode	Orbit	Polarization	Incidence angle at scene centre
2006/04/20	WSS	DSC	HH	22.2
2006/04/26	WSS	DSC	HH	22.2

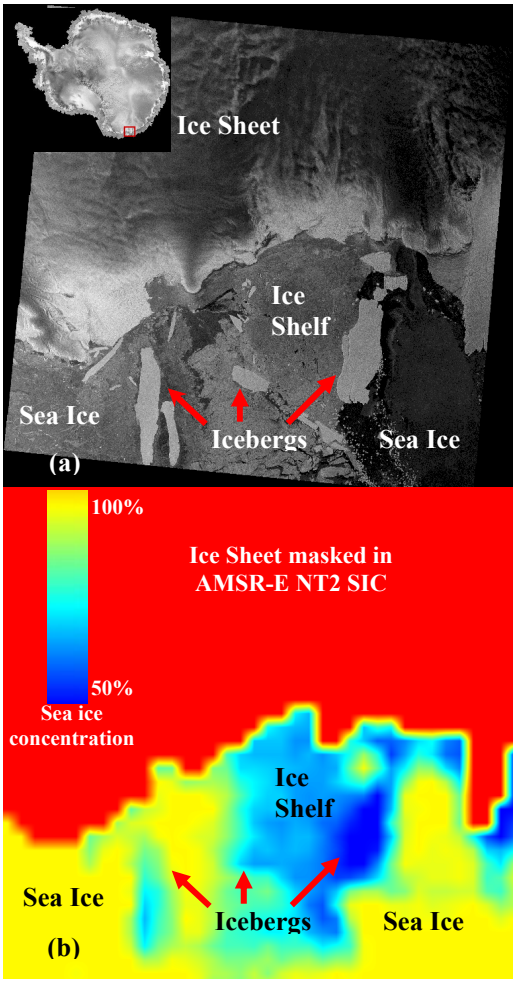

Figure 1. (a) ENVISAT ASAR images of study area obtained on 26 April, 2006. (b) AMSR-E NASA Team2 daily-averaged sea ice concentration image obtained on 26 April, 2006.

classification and digitizing. We calculated the concentration of sea ice, icebergs, and ice shelf from two ASAR images. The overall accuracy of the classification in each ASAR image is 97.4% and 94.4%, respectively (Table 2).

AMSR-E onboard on Aqua is a PM sensor which is composed of 6.9, 10.7, 18.7, 23.8, 36.5, and 89.0 GHz dual polarized channels. AMSR-E provides SIC with 12.5 km resolution by using NT2 algorithm. National Snow and Ice Data Center (NSIDC) provides AMSR-E Brightness Temperature (T_B) and NT2 SIC of daily-averaged, day-time (ascending orbit), and night-time (descending orbit) products. We obtained the AMSR-E

Table 1. Accuracy of the classification of ASAR images.

	User accuracy		Producer accuracy		Overall accuracy
	Ice	Open water	Ice	Open water	
2006/04/20	98.51%	84.12%	98.66%	82.68%	97.40%
2006/04/26	96.35%	86.69%	96.64%	85.67%	94.41%

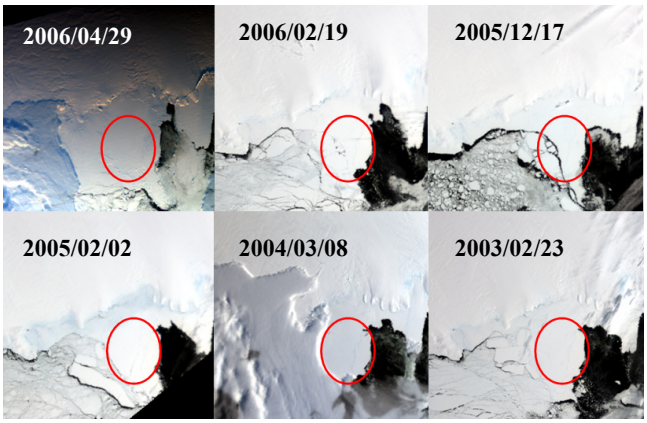

Figure 2. MODIS images obtained in summertime in 2006, 2005, 2004, and 2003. Red circle in each image represents an ice shelf that survived in summertime.

NT2 SIC and the T_B data products of the same dates as the ASAR images (Fig. 1b).

NT2 algorithm identifies ice type A, B, and C, and open water by plotting data in *PR* (polarization ratio) and *GR* (spectral gradient ratio) domain. The *PR* and *GR* is calculated as (Markus and Cavalieri, 2000)

$$PR(v) = \frac{(T_B(v,V) - T_B(v,H))}{(T_B(v,V) + T_B(v,H))} \quad (1)$$

$$GR(v_1 p\ v_2 p) = \frac{(T_B(v_1,p) - T_B(v_2,p))}{(T_B(v_1,p) + T_B(v_2,p))}$$

where v is the channel and p is the polarization. In NT2 algorithm, *PR* (18) and *GR* (37V18V) domain is used to identify sea ice types and open water (Fig. 3). Sea ice has smaller value of both *PR* (18) and *GR* (37V18V) when compared with open water that has high *PR* and *GR*. The *PR* and *GR* of snow layer on ice surface are similar to open water (Markus *et al.*, 2006). In order to classify the ice type that has large surface effect by snow layer (i.e., ice type C), NT2 algorithm uses 89.0 GHz channel.

As the variation of daily temperature can change the radiation property, we excluded pixels of AMSR-E data that have large change in SIC and T_B products. However, sea ice on Antarctic Ocean in this winter season was spatially and temporally stable (Lee and Han, 2008). When observed by the ASAR images, the ocean surface was mostly covered with sea ice with a little open water by narrow cracks.

In the sea ice region, the difference between ASAR SIC and AMSR-E NT2 SIC was very small by 1.4% of RMSE. The NT2 algorithm, however, underestimates SIC on icebergs and ice shelf by 29.5% and 23.3% of RMSE, respectively. To interpret the large deviation of estimation over glacial ice, we analyzed the characteristics of microwave radiation of the glacial ice in *PR* and *GR* domain.

3. GLACIAL ICE ON PR-GR SCATTERGRAM

Fig. 3 shows the scattergram between *PR* (18) and *GR* (37V18V) of sea ice (black dots) and glacial ice (icebergs in blue dots, and ice shelf in blue cross). The vertices of a triangle represent ice type A, ice type B, and open water, respectively. Ice type A in the Antarctic Ocean is similar to first-year ice in the Arctic Ocean. Ice type B, which is similar to multi-year ice in the central Arctic Ocean, has thick snow cover and is mostly found at Weddell Sea. Most sea ice around the Antarctica is ice type A because the sea ice thaws completely during summertime. High

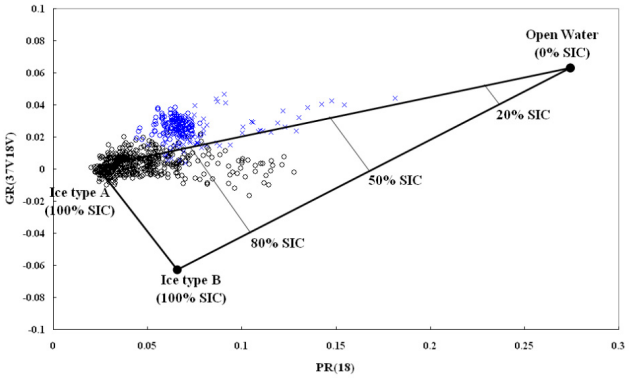

Figure 3. Scattergram between *PR* (18) and *GR* (37V18V) of sea ice (black dots) and glacial ice (icebergs in blue dots and ice shelf in blue cross). The glacial ice forms a unique cluster in *PR* (18) and *GR* (37V18V) domain.

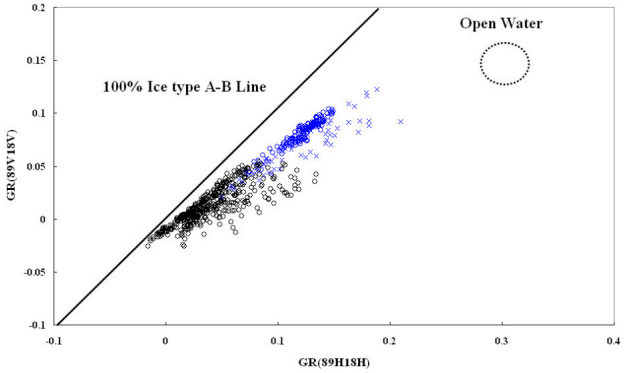

Figure 4. Scattergram between *GR* (89H18H) and *GR* (89V18V) of sea ice (black dots) and glacial ice (icebergs in blue dots and ice shelf in blue cross). The glacial ice forms a unique cluster in *GR* (89H18H) and *GR* (89V18V) domain.

Table 3. Statistics of AMSR-E *PR*s and *GR*s.

		PR (18)	GR (37/18V)	GR (89/18V)	GR (89/18H)
Sea ice	Avg.	0.047	0.006	0.021	0.048
	Std.	0.018	0.005	0.016	0.024
	Max.	0.113	0.022	0.054	0.117
	Min.	0.025	-0.006	-0.015	-0.002
	Mdn.	0.043	0.006	0.020	0.045
Icebergs	Avg.	0.086	0.024	0.067	0.117
	Std.	0.027	0.010	0.024	0.038
	Max.	0.181	0.047	0.123	0.210
	Min.	0.050	0.004	0.021	0.049
	Mdn.	0.076	0.024	0.066	0.112
Ice shelf	Avg.	0.064	0.027	0.083	0.124
	Std.	0.006	0.005	0.011	0.014
	Max.	0.074	0.039	0.104	0.150
	Min.	0.044	0.009	0.047	0.079
	Mdn.	0.065	0.027	0.086	0.125

PR (18) is a typical signature of new ice or snow layer on sea ice that reduces SIC (Cavalieri *et al*., 2006; Markus *et al*., 2006). New ice has similar characteristics with open water because of its thin ice thickness. When sea ice is covered with a snow layer (ice type C), the radiance of 18.7 GHz horizontal polarization reduces so that higher *PR* (18) is calculated than a sea ice without snow cover. *GR* (37V18V) of ice type C has negative value between ice type A and B. The equi-concentration lines of sea ice are parallel to the side of the triangle connecting points of ice type A and B.

The average of *PR* (18) from icebergs and ice shelf were calculated as 0.086 and 0.064, respectively (Table 3), which is larger than the average value of sea ice (0.047). *GR* (37V18V) from icebergs and ice shelf were also higher than sea ice. In general, glacial ice forms a unique cluster in the *GR* (37V18V) - *PR* (18) domain against any other types of ice and open water used in the NT2 algorithm.

Fig. 4 shows the scattergram between *GR* (89H18H) and *GR* (89V18V) of sea ice (black dots) and glacial ice (icebergs in blue dots, and ice shelf in blue cross). The black line is 100% of SIC while the black-circled area corresponds to open water. Glacial ice form a unique cluster in the *GR* (89H18H) and *GR* (89V18V) domain.

GR (89H18H) and *GR* (89V18V) of glacial ice are generally higher than those of sea ice due to the difference of radiation property of glacial ice and sea ice at 89.0 GHz and 18.7 GHz. The T_B of 89.0 GHz channel from glacial ice is warmer than sea ice (Martin *et al*., 2007). Moreover, the T_B of 18.7 GHz channel from glacier ice is smaller than that from sea ice (Jiang *et al*., 2007). This is because 89.0 GHz observes the T_B radiating from air/ice interface or the upper layer of ice while 18.7 GHz can detects radiation from lower ice layer as well. The radiation of 18.7 GHz from the lower glacial ice layer is diffused in the upper ice layers. Therefore the observed T_B of 18.7 GHz from thick glacial ice is generally smaller than that from the relatively thinner sea ice.

Through the analysis of radiation characteristics of glacial ice, we found that glacial ice can be uniquely identified in PR-GR domain apart from other sea ice types and open water used in the NT2 Algorithm.

4. CONCLUSION

We evaluated the AMSR-E NASA Team2 (NT2) sea ice concentration (SIC) in an Antarctic region where glacial ice, such as icebergs and an ice shelf, exists. We found that AMSR-E NT2 algorithm underestimates the sea ice concentration when there are glacial ice by 29.5% for icebergs and 23.3% for ice shelf. Moreover, glacial ice showed higher *PR* (18), *GR* (37V18V), *GR* (89V18V), and *GR* (89HV18H) values than those of sea ice. From the scattergrams of *PR* and *GR*, we found that the characteristics of microwave radiation from glacial ice are quite different from that of sea ice and open water.

We are planning to analyze characteristic of microwave radiation of glacial ice in various seasons and regions, and to improve the accuracy of AMSR-E NT2 algorithm by adding glacial ice concentration (GIC). GIC can also be used for the study of improvement in land-masking of AMSR-E products, iceberg tracking, and monitoring of coastal landform by the movement of glacial ice.

ACKNOWLEDGMENTS

This research was supported by Basic Science Research Program through the National Research Foundation of Korea (NRF) funded by the Ministry of Education, Science and Technology (No. 2010-0009465).

REFERENCES

Andersen, S., L. Kaleschke, G. Heygster, and L. T. Pedersen, 2007. Intercomparison of passive microwave sea ice concentration retrievals over the high-concentration Arctic sea ice, *Journal of Geophysical Research*, doi:10.1029/2006JC003543.

Cavalieri, D. J., P. Gloersen, C. L. Parkinson, J. C. Comiso, and H. J. Zwally, 1997. Observed hemispheric asymmetry in global sea ice changes, *Science*, 278(5340), pp. 1104-1106.

Cavalieri, D. J., T. Markus, D. K. Hall, A. J. Gasiewski, M. Klein, and A. Ivanoff, 2006. Assessment of EOS Aqua AMSR-E arctic sea ice concentration using Landsat-7 and airborne microwave imagery, *IEEE Transactions on Geoscience and Remote Sensing*, 44(11), pp. 3057-3069.

Han, H., and H. Lee, 2007. Comparative study of KOMPSAT-1 EOC images and SSM/I NASA Team sea ice concentration of the Arctic, *Korean Journal of Remote Sensing*, 23(6), pp. 507-520.

Haykin, S., E. O. Lewis, R. K. Raney, and J. R. Rossiter, 1994. *Remote Sensing of Sea Ice and Icebergs*. John Wiley & Sons, Inc., New York, pp. 43-44.

Jiang, L., J. Shi, S. Tjuatja, J. Dozier, K. Chen, and L. Zhang, 2007. A parameterized multiple-scattering model for microwave emission from dry snow, *Remote Sensing of Environment*, 111(2-3), pp. 357-366.

Lee, H., and H. Han, 2008. Evaluation of SSM/I and AMSR-E sea ice concentrations in the Antarctic spring using KOMPSAT-1 EOC imagery, *IEEE Transactions on Geoscience and Remote Sensing*, 46(7), pp. 1905-1912.

Markus, T., and D. J. Cavalieri, 2000. An enhancement of the NASA Team sea ice algorithm, *IEEE Transactions on Geoscience and Remote Sensing*, 38(3), pp. 1387-1398.

Markus, T., D. J. Cavalieri, A. J. Gasiewski, M. Klein, J. A. Maslanik, D. C. Powell, B. B. Stankov, J. C. Stroeve, and M. Sturm, 2006. Microwave signatures of snow on sea ice: Observations, *IEEE Transactions on Geoscience and Remote Sensing*, 44(11), pp. 3081-3090.

Martin, S., R. S. Drucker, and R. Kwok, 2007. The areas and ice production of the western and central Ross Sea polynyas, 1992-2002, and their relation to the B-15 and C-19 iceberg events of 2000 and 2002, *Journal of Marine Systems*, 68(1-2), pp. 201-214.